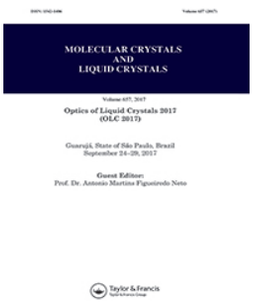

Molecular Crystals and Liquid Crystals

ISSN: 1542-1406 (Print) 1563-5287 (Online) Journal homepage: https://www.tandfonline.com/loi/gmcl20

Plasmonic nanoantennas with liquid crystals for nanocrystal fluorescence enhancement and polarization selectivity of classical and quantum light sources

Svetlana G. Lukishova, Andreas C. Liapis, Huiqing Zhu, Eric Hebert, Kevin Kuyk, Saumya Choudhary, Robert W. Boyd, Ziyue Wang & Luke J. Bissell

To cite this article: Svetlana G. Lukishova, Andreas C. Liapis, Huiqing Zhu, Eric Hebert, Kevin Kuyk, Saumya Choudhary, Robert W. Boyd, Ziyue Wang & Luke J. Bissell (2017) Plasmonic nanoantennas with liquid crystals for nanocrystal fluorescence enhancement and polarization selectivity of classical and quantum light sources, Molecular Crystals and Liquid Crystals, 657:1, 173-183, DOI: 10.1080/15421406.2017.1404420

To link to this article: https://doi.org/10.1080/15421406.2017.1404420

Published online: 18 Jan 2018.

MOLECULAR CRYSTALS AND LIQUID CRYSTALS
2017, VOL. 657, 173–183
https://doi.org/10.1080/15421406.2017.1404420

Taylor & Francis
Taylor & Francis Group

Plasmonic nanoantennas with liquid crystals for nanocrystal fluorescence enhancement and polarization selectivity of classical and quantum light sources

Svetlana G. Lukishova[a], Andreas C. Liapis[a,*], Huiqing Zhu[a], Eric Hebert[a], Kevin Kuyk[a], Saumya Choudhary[a], Robert W. Boyd[a,**], Ziyue Wang[b,***], and Luke J. Bissell[c]

[a]The Institute of Optics, University of Rochester, Rochester, New York, USA; [b]Department of Physics and Astronomy, University of Rochester, New York, USA; [c]U.S. Air Force Research Laboratory, Wright-Patterson Air Force Base, Ohio, USA

ABSTRACT

We discuss plasmonic nanoantennas for emitter fluorescence enhancement and wavelength tunability of plasmonic resonance using liquid crystals. The results of numerical modeling of a plane wave scattered by bowtie nanoantennas in isotropic liquid crystal media with different refractive indexes are presented for two plasmonic materials. Experimental results are reported on fabricated gold bowtie nanoantenna arrays by high-precision electron-beam lithography. Photon antibunching from nanocrystal quantum dot within a bowtie nanoantenna gap was obtained, proving nonclassical behavior of light from such a source. In addition, the first results towards gap/patch nanoantennas with single emitters in liquid crystal hosts as well as photon antibunching are reported for nanodiamonds with NV-color-centers dispersed in nematic liquid crystal hosts. Depending on nanocrystal concentration our results can find applications in displays, organic light-emitting diodes, microlasers, and single photon sources for secure quantum communication.

KEYWORDS

Antibunching; bowtie nanoantennas; colloidal nanocrystal quantum dots; liquid crystals; NV-center nanodiamonds

Introduction

Fluorescence enhancement and achieving definite polarization of emitter fluorescence in planar aligned liquid crystal structures are well known [1–13]. 1D-photonic bandgap cholesteric liquid crystal lasers [14–22] comparable in size with diode lasers, with continuous wide spectrum tunability and a relatively large coherence length can find applications in biomedical and environment sensing as well as in display technology. Single-emitter doped liquid crystals are also used for single (antibunched) photon sources with definite linear [1–2, 4–5, 12–13] and circular [1–2, 5–7, 23–30] polarizations that are important for secure, long-distance quantum communication. Antibunching is separation of all photons in time and cannot be obtained from classical light sources [31–33]. For photon antibunching the second-order coherence

CONTACT Svetlana G. Lukishova sluk@lle.rochester.edu The Institute of Optics, University of Rochester, Rochester, NY 14627-0186, USA.

Color versions of one or more of the figures in the article can be found online at www.tandfonline.com/gmcl.

*Now at Wellman Center for Photomedicine, Massachusetts General Hospital, Harvard Medical School, Cambridge, MA 02139, USA.

**Also University of Ottawa, Ontario, K1N 6N5 Canada.

***Now at Stanford University, CA 94305, USA.

function [31–32, 34]

$$g^{(2)}(t) = \frac{\langle I(t)I(t+\tau)\rangle}{\langle I(\tau)\rangle^2}, \tag{1}$$

should have a minimum at interphoton time $t = 0$. Here $I(t)$ is intensity, t and τ are two moments of time, and brackets denote time averaging.

In this paper we consider the advantages of using liquid crystal hosts with plasmonic nanoantennas. From all photonic structures plasmonic nanoantennas provide both the highest reported emission rate enhancements and the highest photon flux increase from emitters [1, 35–39]. The optical properties of the metal structures are strongly affected by surface plasmon polaritons, i.e. electromagnetic excitations propagating at the interface between a dielectric and a metal [40–45]. They arise from the coupling of electromagnetic fields to oscillations of the metal's electron plasma. A prominent example is metal surface enhanced Raman scattering: there enhancement factors of 10^{14} have been observed [46].

Plasmonic nanoantennas [42–45] serve to spatially enhance and localize fields, and modify the excitation rate and the radiative decay rate when placed close to emitters. But they can also cause undesirable losses, leading to an increase in the non-radiative decay rates of these emitters. This interplay of rates can lead to a strong modification of the emission characteristics of emitters. The key to having efficient antennas for fluorescence enhancement is to minimize non-radiative losses in the metal (quenching). Simulations and experiments, see, e.g., Refs. [43–44, 47] showed that for short distances between the emitter and a metal antenna, the decrease of quantum yield wins over the increase of the excitation rate thereby quenching the fluorescence of the emitter. Both the experiment and the theory showed that the fluorescence enhancement reaches a maximum at a several nanometer distance between the emitter and the metal. For shorter distances fluorescence is quenched. The authors of Refs [48–50] showed calculations that, using different nanoantenna structures manufacturable with today's nanotechnology and with improved technology [50], it is possible to increase the radiative decay rate by three to five orders of magnitude. Two types of nanoantennas are most promising: bowtie [1, 30, 35, 51–55] and gap/patch [36–39]. Bowtie nanoantenna consists of two or more metal triangle tips separated by a nanometer-sized gap (Figure 1). In a gap/patch nanoantenna the emitters are situated in a vertical dielectric gap between a metal nanoparticle of a given shape (nanorod, cube, triangle, etc.) and a metal film.

Placing nanoantenna in liquid crystal medium can provide wavelength tunability of plasmonic resonance by temperature and applied electric field. In addition, liquid crystals can limit the exposure of silver nanostructures to ambient air [23] that destroys them.

The structure of this paper is as follows. Section 1 is devoted to numerical modeling of a plane wave scattered by a bowtie nanoantenna on a glass substrate immersed in isotropic liquid crystal media with different refractive indexes (section 1.1 – gold bowtie nanoantenna, section 1.2 – silver bowtie nanoantenna). In sections 2 and 3 experimental setup and sample preparation are described. In section 4.1 photon antibunching from nanocrystal quantum dot within bowtie nanoantenna is reported. Section 4 also describes our results towards gap/patch nanoantennas with nitrogen vacancy (NV) color centers in nanodiamonds: photon antibunching from NV-center nanodiamonds in liquid crystal host (section 4.2) and fluorescence enhancement from NV-center diamonds in liquid crystal host with dispersed silver nanorods (section 4.3). Section 5 concludes the paper.

1. Numerical modeling of bowtie plasmonic nanoantenna in liquid crystal host

Numerical modeling of bowtie nanoantennas was carried out using Lumerical Solutions software with a finite difference time domain (FTDT) method. Figure 1, left shows the coordinates that were used in numerical modeling. Nanoantenna was placed on a thick glass substrate and was immersed to the liquid crystal medium. Figure 1, right shows typical electric field distributions near a bowtie nanoantennas (two polarizations together) with the incident polarization of a plane wave along the bowtie axis (top) and perpendicular to the bowtie axis (bottom).

Modeling liquid crystal medium we carried out calculations for refractive indexes n = 1.4, 1.5, 1.6 and 1.7 for incident polarization parallel to a bowtie axis (X-polarization) and n = 1.44 and 1.5 for incident polarization perpendicular to a bowtie axis (Y-polarization). Two plasmonic materials were used: gold and silver.

1.1. Gold bowtie nanoantennas

Figure 2 (top) shows spectral dependence of scattering cross-sections of a gold bowtie nanoantenna with an incident plane wave for incident polarization parallel to the bowtie axis (top figure) and perpendicular to the bowtie axis (bottom). Inserts show refractive indexes of liquid crystals n_{LC} and scattered wave polarizations (X or Y).

1.2. Silver bowtie nanoantennas

The similar spectral dependences of scattering cross-sections as in section 1.1 are presented in Figure 3 for silver bowtie nanoantennas with plasmonic resonances at shorter wavelengths than for gold. Inserts show refractive indexes of liquid crystals n_{LC} and scattered wave polarizations (X or Y).

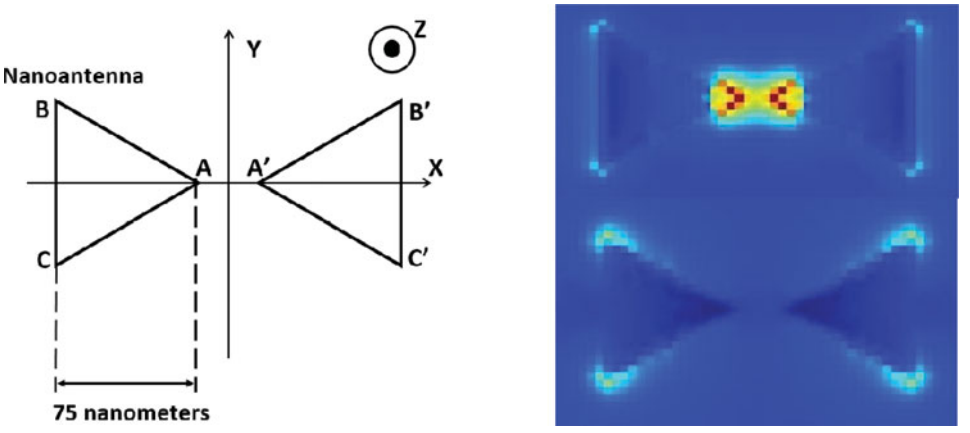

Figure 1. LEFT: The plot of a bowtie nanoantenna showing the coordinates that were used in numerical modeling. The polarization along the y-axis is defined as "vertical polarization," and the polarization along the x-axis is defined as "horizontal polarization." The z-axis is thus defined as the direction perpendicular to the paper. Each triangle is an equilateral triangle, with a 75 nm height and 30 nm gap. RIGHT: Electric field distribution near a typicalbowtie nanoantenna (two polarizations together) with the incident polarization of a plane wave along a bowtie axis (top) and perpendicular to a bowtie axis (bottom).

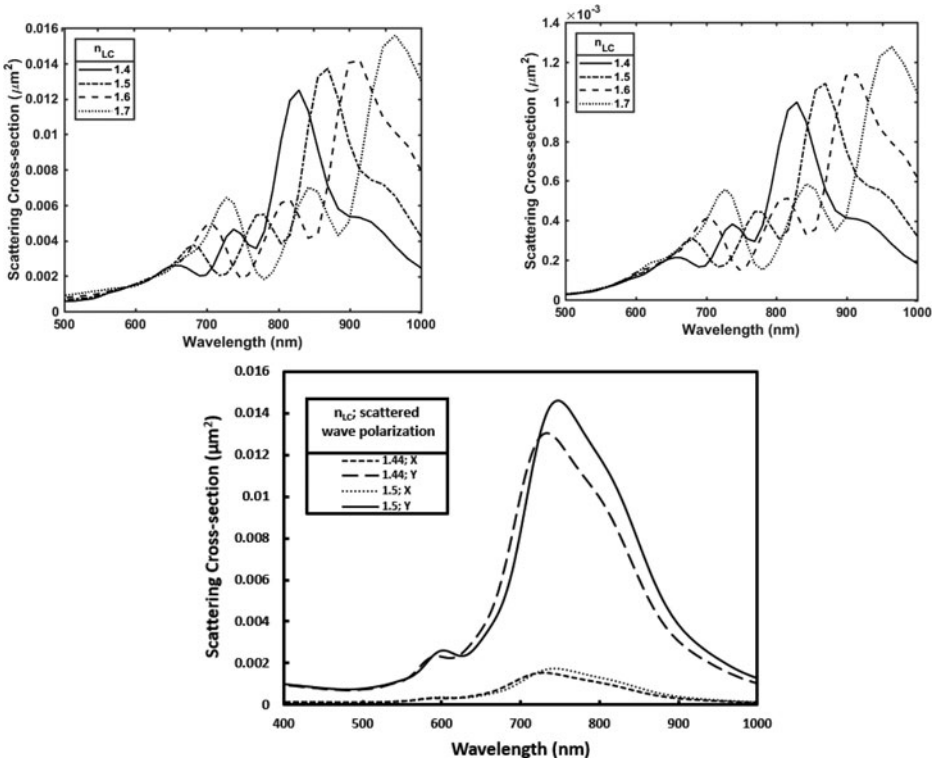

Figure 2. Spectral dependence of scattering cross-sections of a gold bowtie nanoantenna for an incident plane wave. TOP: Incident polarization is parallel to the bowtie axis (X-polarization). The upper left figure shows data for only X-polarized scattered light, upper right figure shows data for only Y-polarized scattered light. Inserts show refractive indexes of liquid crystals n_{LC} for different curves. BOTTOM: Incident polarization is perpendicular to a bowtie axis.

2. Experimental setup

The experimental setup consists of a home-built confocal fluorescence microscope (Figure 4, left) based on a Nikon TE2000-U inverted microscope with a high numerical aperture N.A. = 1.35, oil-immersion objective that focuses a pulsed or cw-laser beam on a sample with nanoantennas and emitters. The sample is mounted on a piezo-translation stage for raster scanning the sample through the focused laser beam. Fluorescence light is collected by the same objective. A dichroic mirror reflects laser light and transmits fluorescence light. Interference filters with $\sim$ 11 orders of magnitude attenuation further reject the excitation laser light. Figure 4, left shows a spectrometer (Acton SP-2500i of Princeton Instruments) with a low-light level EM-CCD (Andor Technologies, iXon DV887) for spectral measurements at a single-photon level.

A general schematic of this experimental setup is presented in Figure 4, right. In addition to a confocal microscope, a Hanbury Brown and Twiss intensity interferometer (correlator) [56] is used. It consists of a nonpolarizing beamsplitter, two single-photon counting detectors (thermoelectrically cooled Perkin Elmer silicon avalanche photodiode modules (APDs) AQR-14 for visible and near-IR light), and start-stop electronics (TimeHarp 2000, PicoQuant) to measure time intervals between two consecutive photons in pairs to prove photon antibunching. The histogram can be built showing how many second photons $c\,(\tau)$ in photon pairs appear after first photons at definite time interval τ. To obtain the value of $g^{(2)}(\tau)$ which

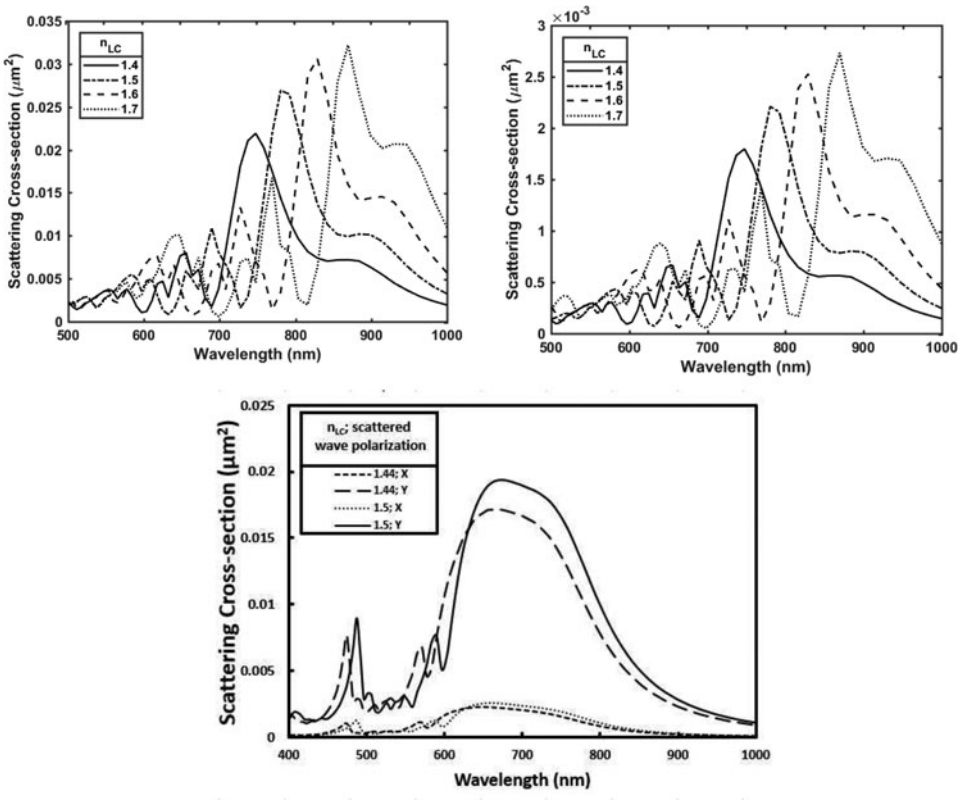

Figure 3. Spectral dependence of scattering cross-sections of a silver bowtie nanoantenna for an incident plane wave. TOP: Incident polarization is parallel to the bowtie axis (X-polarization). The upper left figure shows data for only X-polarized scattered light, upper right figure shows data for only Y-polarized scattered light. Inserts show refractive indexes of liquid crystals n_{LC} for different curves. BOTTOM: Incident polarization is perpendicular to a bowtie axis.

is proportional to coincidence count $c(\tau)$, normalization is required. The normalization can be deduced by calculation of $g^{(2)}(\tau) = c(\tau)/(I_1 I_2 \Delta t T)$, where I_1 and I_2 are the mean intensities on start and stop channels, Δt is the time resolution, and T is the total acquisition time [57]. Time resolution was restricted by APDs (500 ps) and acquisition time varied from 1 to 20 minutes depending on single emitter fluorescence intensity.

3. Sample preparation

Gold bowtie nanoantennas

Gold bowtie nanoantennas (Figure 5) were fabricated using high-precision electron-beam lithography on ~120-μm-thick glass coverslips with 1 inch × 1 inch dimensions that were coated with ~40 nm of ITO to serve as a charge conduction layer. The base dose was 1000 nC/cm^3. The dose modulations were from 0 to 105%. Bilayer of 495 k/950 k-molecular-weight poly(methyl methacrylate) was spun onto the ITO and patterned using a JEOL JBX 9500 100 Kev lithography tool (Cornell NanoScale Facility). After exposure, the resist was developed in a IPA:MIBK (3:1) solution. Prior to gold deposition, the samples were exposed to an oxygen plasma at 60 W for 120 seconds. A 5 nm titanium adhesion layer was deposited

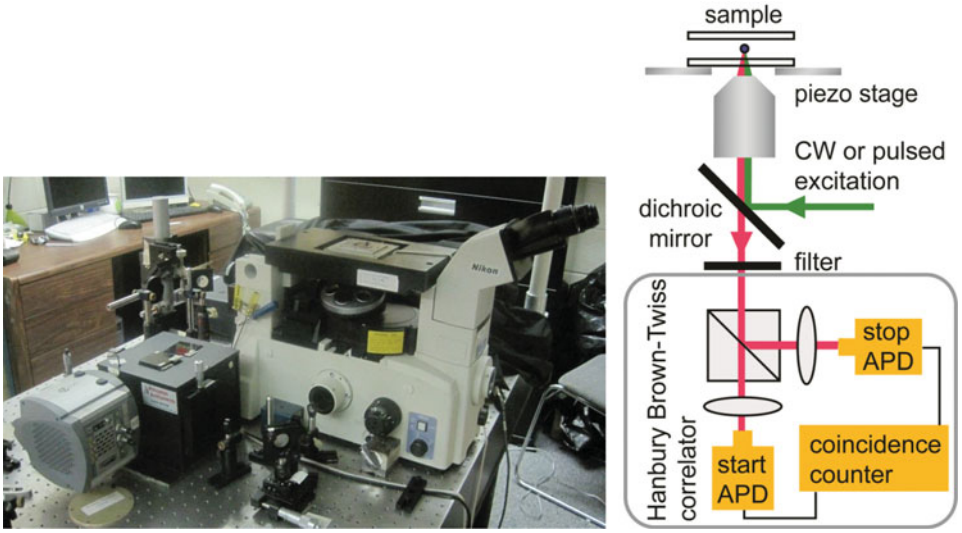

Figure 4. LEFT: Photograph of an experimental setup for a confocal fluorescence microscopy of single-emitters in nanoantennas, spectral and photon antibunching measurements. RIGHT: Schematic of this experimental setup (APD is single-photon counting avalanche photodiode module). A Hanbury Brown and Twiss correlator is used for photon antibunching measurements.

by electron-beam evaporation (the CVC SC4500 evaporator) followed by 30 nm of gold. Pattern transfer was achieved by lift-off in acetone during more than 8 hours.

We prepared arrays of bowtie nanoantennas with equilateral triangles with 75 nm height with different gaps from 16 to 60 nm.

Colloidal nanocrystal quantum dots

We used colloidal nanocrystal CdSeTe quantum dots (NQDs) with ZnS shell from Invitrogen (Qdot 800 ITK organic) with fluorescence maximum near 790 nm. NQDs had elliptical shape and with streptavidin conjugate their size was 15–20 nm. They were spin-coated from solution to the sample surface with bowtie nanoantenna arrays.

Nanodiamonds with NV-color centers

Two types of nitrogen vacancy (NV) nanodiamonds dispersed in a deionized water with maximum fluorescence wavelength near 650 nm were used in different experiments: (1) 30–50 nm

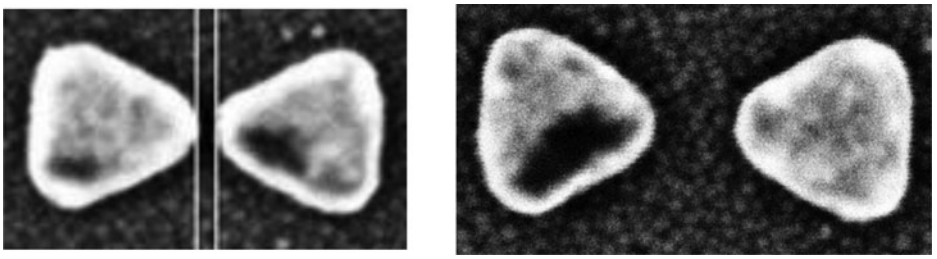

Figure 5. SEM-micrographs of typical fabricated gold bowtie nanoantenna arrays with 16 nm (left) and 60 nm (right) gaps. Electron microscopy was made by Z. Shi.

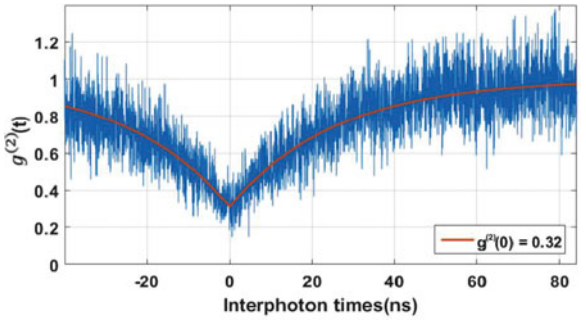

Figure 6. Antibunching histogram of fluorescence from a single CdSe/CdTe nanocrystal quantum dot (790 nm fluorescence maximum, 633 nm excitation wavelength) within a 30 nm gap gold bowtie nanoantenna.

in diameter purchased from Microdiamant AG, Switzerland and (2) 40-nm in diameter purchased from Adamas Nanotechnologies.

Silver nanorods

Monodispersed pentagonal shaped ~100 nm silver nanorods in aqueous solution (Sciventions, Toronto) with the longitudinal mode of plasmonic resonance near 650 nm were used to enhance fluorescence of NV-center nanodiamonds in liquid crystal hosts.

Liquid crystals

In our experiments we used monomeric nematic liquid crystals mixture E7 (Merck). In some experiments chiral agent CB 15 (Merck) was added.

4. Experimental results

4.1. Photon antibunching from nanocrystal quantum dot within bowtie nanoantenna

Figure 6 shows fluorescence antibunching histogram of NQD within a gold bowtie nanoantenna. After spin coating of solution with NQDs some NQDs were located within the gaps of nanoantennas (Figure 7, left). In one sample several NQDs appeared to be in a gap. Antibunching with $g^{(2)}$ from 0.15 to 0.7 was observed for such NQDs, showing nonclassical behavior of the source. Figure 7 shows also a weak photoluminescence (in comparison with NQDs fluorescence) from gold nano-antennas (periodic array).

Figure 7, right presents "time traces" of fluorescence of a single NQD within a bowtie nanoantenna which show NQD blinking (changing intensity of its fluorescence in time).

4.2. Photon antibunching of NV-center nanodiamonds in liquid crystal host

Photon antibunching in liquid crystal host was obtained for NV-center nanodiamonds in liquid crystal host. Figure 8, left shows antibunching histogram from a single NV-color center dispersed in a monomeric cholesteric liquid crystal host (E7 and CB15 mixture) with 514-nm, cw-laser excitation. The value of $g^{(2)}(0) = 0.74$. The spectrum of NV-center nanodiamond in this liquid crystal host is presented in Figure 8, right.

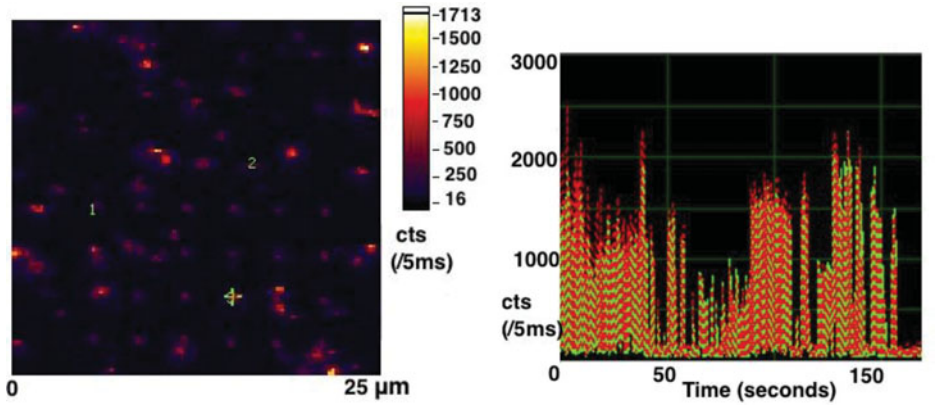

Figure 7. LEFT: Confocal fluorescence microscopy raster scan image of weak photoluminescence of a typical nanoantenna array and single CdSe/CdTe nanocrystal quantum dots spin coated on this sample (633 nm laser excitation). Cross shows a position of a quantum dot within a nanoantenna with photon antibunching (Figure 6). RIGHT: Time traces of fluorescence of a single nanocrystal quantum dot within a gold bowtie nanoantenna showing quantum dot blinking.

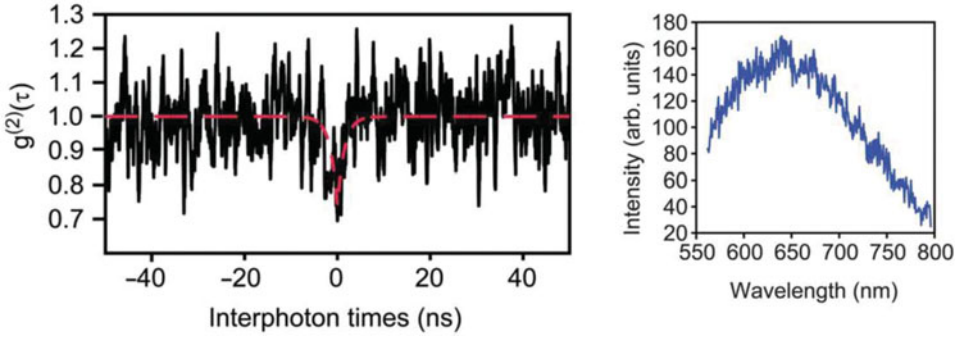

Figure 8. LEFT: Antibunching histogram of fluorescence from a single NV-color center in nanodiamonds dispersed in a monomeric cholesteric liquid crystal host (514 nm, cw-excitation was used). RIGHT: Fluorescence spectrum of the NV-color center in nanodiamonds in a monomeric cholesteric liquid crystal host.

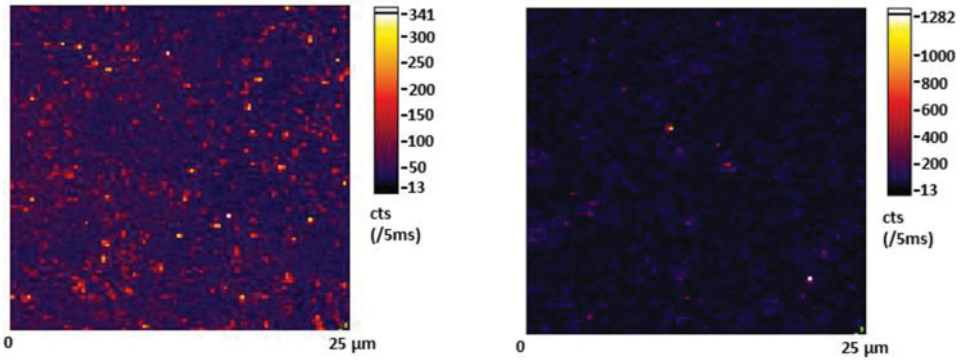

Figure 9. Confocal microscope raster scan images of fluorescence from NV-color-centers in nanodiamonds dispersed in E7 nematic liquid crystals. LEFT: Without silver nanorods (maximum count rate is ~340 counts/5 msec); RIGHT: With added silver nanorods (maximum count rate increased up to ~1280 counts/5 msec).

4.3. Fluorescence enhancement of NV-center nanodiamond in liquid crystal with dispersed plasmonic nanorods

Figure 9, left shows raster scan images of fluorescence of single or few NV-centers in nanodiamonds dispersed in E7 liquid crystal host. Even maximum count rate did not exceed 340 counts/5 msec. After addition to this material 100-nm silver nanorods brightness of NV-centers significantly enhanced (up to 1280 counts/5 msec as shown in Figure 9, right).

5. Conclusion

This paper demonstrates the advantages of using plasmonic nanoantennas with a liquid crystal environment on the example of bowtie nanoantennas for the first time. Numerical modeling showed shifting plasmonic resonance of nanoantenna to the longer wavelengths with increasing refractive index of liquid crystal medium. This tunability can be made by temperature or electric field variation. Additionally, liquid crystals protect silver from ambient air.

We fabricated gold bowtie nanoantenna arrays by high-precision electron beam lithography and observed photon antibunching of NQD within a gap of nanoantenna that is evidence of a nonclassical behavior of the source. An example of photon antibunching from NV-color center nanodiamonds in liquid crystal hosts was obtained as well.

Our next steps will be experiments with wavelength tunability of fluorescence of single emitter nanocrystals (NQDs and NV-nanodiamonds) in bowtie and gap nanoantennas with silver rods in liquid crystal hosts. We also will use glassy liquid crystal oligomers [58–59] to select a fixed combination of nanoantenna parameters and refractive index of the medium for each particular nanoemitter.

Acknowledgments

University of Rochester (UR) Laboratory for Laser Energetics liquid crystal clean room facility, Cornell Nanoscale and UR NanoCenter facilities were used. We thank K. Marshall for his advice, Z. Shi for some preliminary experiments and his help, D. Mihaylova for assistance in sample preparation, and R. Bi and T. Jacobs for assistance in antibunching measurements.

Funding

This research was supported by the NSF award EEC 1343673 (SGL).

References

[1] Lukishova, S. G., & Bissell, L. J. (submitted). *Advances in Quantum Photonics: from the First Single-photon and Nonlinear Optical Experiments to Modern Quantum Photonics*, Springer Series in Optical Sciences.
[2] Lukishova, S. G., Liapis, A. C., Bissell, L. J., Gehring, G. M., & Boyd, R. W. (2014). *Liquid Crystal Reviews.*, *2*, 111.
[3] Schmidtke, J., & Stille, W. (2003). *Europ. Phys. J.*, *31*, 179.
[4] Lukishova, S. G., Schmid, A. W., Knox, R. P., Freivald, P., McNamara, A., Boyd, R. W., Stroud, C. R. Jr., & Marshall, K. L. (2006). *Molec. Cryst. Liq. Cryst.*, *454*, 1.
[5] Lukishova, S. G., Bissell, L. J., Stroud, C. R. Jr., & Boyd, R. W. (2010). *Optics and Spectroscopy.*, *108*, 417.
[6] Lukishova, S. G., Bissel, L. J., Winkler, J., & Stroud, C. R. Jr. (2012). *Opt. Lett.*, *37*, 7, 1259.
[7] Bissell, L. J. (2011). *Experimental Realization of Efficient, Room-Temperature Single-Photon Sources with Definite Circular and Linear Polarization*, University of Rochester: Rochester, NY.

[8] Chen, S. H., Katsis, D., Schmid, A. W., Mastrangelo, J. C., Tsutsui, T., & Blanton, T. N. (1999). *Nature.*, *397*, 506.
[9] Katsis, D., Schmid, A. W., & Chen, S. H. (1999). *Liq. Cryst.*, *26*, 181.
[10] Bobrovsky, A. Y., Boiko, N. I., Shibaev, V. P., & Wendorff, J. H. (2003). *Adv. Mater.*, *15*, 3, 282.
[11] Du, T., Schneider, J., Srivastava, A. K., Susha, A. S., Chigrinov, V. G., Kwok, H. S., & Rogach, A. L. (2015). *ACS Nano.*, *9*, 11049.
[12] Pelliser, L., Manceau, M., Lethiec, C., Coursault, D., Vezzoli, S., Leménager, G., Coolen, L., DeVittorio, M., Pisanello, F., Carbone, L., Maitre, A., Bramati, A., & Lacaze, E. (2015). *Adv. Funct. Mater.*, *25*, 1719.
[13] Manceau, M. (2014). *Single CdSe/CdS dot-in-rods fluorescence properties*, University of Pierre et Marie Curie: Paris, France.
[14] Il'chishin, I., Tikhonov, E., Tishchenko, V., & Shpak, M. (1978). *JETP Lett.*, *32*, 24.
[15] Ilchishin, I. P., & Tikhonov, E. A. (2015). *Progress in Quantum Electronics.*, *41*, 1.
[16] Kopp, V. I., Fan, B., Vithana, H. K. M., & Genack, A. Z. (1998). *Opt. Lett.*, *23*, 1707.
[17] Palffy-Huhoray, P., Cao, W., Moreira, M., Taheri, B., & Munoz, A. (2006). *Phil. Transact. A Math. Phys. Eng. Sci.*, *364*, 2747.
[18] Coles, H., & Morris, S. (2010). *Nature Photonics.*, *4*, 678.
[19] Blinov, L. M., & Bartolino, R. (2010). *Liquid Crystal Microlasers*, Transworl Res. Network: Trivandrum, India.
[20] Chilaya, G., Chanishvili, A., petriashvili, G., Barberi, R., De Santo, P., & Matranga, M. A. (2011). *Scient. Research, Materials Sciences and Applications.*, *2*, 116.
[21] Dolgaleva, K., Wei, S. K. H., Lukishova, S. G., Chen, S. H., Schwertz, K., & Boyd, R. W. (2008). *JOSA B.*, *25*, 1496.
[22] Wei, S. K. H., Chen, S. H., Dolgaleva, K., Lukishova, S. G., & Boyd, R. W. (2009). *Appl. Phys. Lett.*, *94*, 041111.
[23] Lukishova, S. G., Schmid, A. W., McNamara, A. J., Boyd, R. W., & Stroud, C. R. (2003). *IEEE J. Select. Top. Quantum Electron.*, *9*, 6, 1512.
[24] Lukishova, S. G., Schmid, A. W., Supranowitz, C. M., Lippa, N., McNamara, A. J., Boyd, R. W., & Stroud, C. R. Jr. (2004). *J. Mod. Opt.*, *51*, 9, 1535.
[25] Lukishova, S. G., Schmid, A. W., Knox, R., Freivald, P., Bissell, L., Boyd, R. W., Stroud, C. R., Jr, & Marshall, K. L. (2007). *J. Mod. Opt.*, *54*, iss. 2 & 3, 417.
[26] Lukishova, S. G., Bissell, L. J., Menon, V. M., Valappil, N., Hahn, M. A., Evans, C. M., Zimmerman, B., Krauss, T. D., Stroud, C. R. Jr., & Boyd, R. W. (2009). *J. Mod. Opt.*, *56*, 167.
[27] Lukishova, S. G. (2012). *Mol. Cryst. Liq. Cryst.*, *559*, 127.
[28] Lukishova, S. G., Winkler, J. M., & Bissell, L. J. (2014). *Mol. Cryst. Liq. Cryst.*, *595*, 98.
[29] Lukishova, S. G., Winkler, J. M., Bissell, L. J., Mihaylova, D., Liapis, A. C., Shi, Z., Goldberg, D., Menon, V. M., Boyd, R., Chen., G., & Prasad, P. N. (2014). *Emerging Technologies in Security and Defence II and Quantum-Physics-Based Information Security III*, Gruneisen, M. T., Dusek, M., Rarity, J. G., et al. (Eds.), *Proceedings SPIE*, Vol. *9254*, Article Number: UNSP 925405.
[30] Lukishova, S. G., Winkler, J. M., Mihaylova, D., Liapis, A., Bissell, L. J., Goldberg, D., Menon, V. M., Shi, Z., Boyd, R. W., Chen, G., & Prasad, P. (2015). *J. Physics, Conf. Ser.*, *594*, Article Number: 012005.
[31] Mandel, L., & E. Wolf, E. (1995). *Optical Coherence and Quantum Optics*. Cambridge University Press.
[32] Walls, D. F. (1979). *Nature.*, *280*, 451.
[33] Paul, H. (1982). *Rev. Mod. Phys.*, *54*, 1061.
[34] Glauber, R. J. (1963). *Phys. Rev.*, *130*, 2529.
[35] Kinkhabwala, A., Yu, Z., Fan, S., Avlasevich, Y., Müllen, K., & Moerner, W. E. (2009). *Nat. Photonics.*, *3*, 654.
[36] Akselrod, G. M., Argyropoulos, C., Hoang, T. B., Ciracì, C., Fang, C., Huang, J., Smith, D. R., & Mikkelsen, M. H. (2014). *Nat. Photonics.*, *8*, 835.
[37] Hoang, T. B., Akselrod, G. M., Argyropoulos, C., Huang, J., Smith, D. R., & Mikkelsen, M. R. (2015). *Nat. Commun.*, *6*, 7788.
[38] Rose, A., Hoang, T. B., McGuire, F., Mock, J. J., Ciracì, C., Smith, D. R., & Mikkelsen, M. H. (2014). *Nano Lett.*, *14*, 4797.

[39] Eliseev, S. P., Vitukhnovsky, A. G., Chubich, D. A., Kurochkin, N. S., Sychev, V. V., & Marchenko, A. A. (2016). *JETP Letters.*, *103*, No. 2, 82.
[40] Maier, S. A. (2007). *Plasmonics: Fundamentals and Applications*, Springer Science & Business Media.
[41] Klimov, V. (2014). *Nanoplasmonics*. CRC Press.
[42] Agio, M., & Alù, A. (2013). *Optical Antennas*, Cambridge University Press: Cambridge, UK.
[43] Bharadwaj, P. (2012). *Antenna-coupled photoemission from single quantum emitters*, *Ph.D. Thesis*, University of Rochester: Rochester, NY.
[44] Bharadwaj, P., Deutsch, B., & Novotny, L. (2009). *Adv. Opt. Photonics.*, *1*, 438.
[45] Novotny, L., & Van Hulst, N. (2011). *Nat. Photonics.*, *5*, 83.
[46] Moskovits, M. (1985). *Mod. Phys.*, *57*, 783.
[47] Anger, P., Bharadwaj, P., & Novotny, L. (2006). *Phys. Rev. Lett.*, *96*, 113002.
[48] Rogobete, L., Kaminski, F., Agio, M., & Sandoghdar, V. (2007). *Opt. Lett.*, *32*, 1623.
[49] Agio, M. (2012). *Nanoscale.*, *4*, 692.
[50] Fauraud, V., Regmi, R., Winkler, P. M., Alexander, D. T. L., Rigneault, H., van Hulst, N. F., García-Parajo, M. F., Wenger, J., & Brugger, J. (2017). *Nano Lett.*, *17*(3), 1703.
[51] Fromm, D. P., Sundaramurthy, A., Schuck, P. J., Kino, G., & Moerner, W. E. (2004). *Nano Lett.*, *4*(5), 957.
[52] Schuck, P. J., Fromm, D. P., Sundaramurthy, A., Kino, G. S., & Moerner, W. E. (2005). *Phys. Rev. Lett.*, *94*, 017402.
[53] Kaniber, M., Schraml, K., Regler, A., Bartl, J., Glashagen, G., Flassig, F., Wierzbowski, J., & Finley, J. J. (2016). *Scientific Reports.*, *6*, Article Number 23203.
[54] Sharac, N., Sharma, H., Veysi, M., Sanderson, R. N., Khine, M., Capolino, F., & Ragan, R. (2016). *Nanotechnology.*, *27*(10), 105302.
[55] Wang, Q., Liu, L., Wang, Y., Liu, P., Jiang, H., Xu, Z., Ma, Z., Oren, S., Chow, E. K. C., Lu, M., & Dong, L. (2015). *Scientific Reports.*, *5*, 18567.
[56] Brown, R. H., & Twiss, R. Q. (1956). *Nature.*, *177*, 27.
[57] Messin, G., Hermier, J. P., Giacobino, E., Desbiolles, P., & Dahan, M. (2001). *Opt. Lett.*, *26*, 1891.
[58] Lukishova, S. G., & Schmid, A. W. (2006). *Molec. Cryst. Liq. Cryst.*, *454*, 15.
[59] Bunning, T. J., & Kreuzer, F.-H. (1995). *Trends in Polym. Sci.*, *3*(10), 318.